Journal of Functional Materials and Applied Engineering

Research Paper

Degradation performance and mechanisms of UV_{254}/O_3 against multi-component emerging contaminants at trace levels in water

Hugo Lefevre[1,*], Alice Dupont[1], Aisha Khan[2]

[1] Institut des Matériaux Poreux de Paris, ESPCI Paris, CNRS, PSL University, Paris, France
[2] Department of Computer Information Systems, Eastern Michigan University, Ypsilanti, Michigan, USA
*Corresponding author: H.C.Lefevre@ens.psl.eu; AliceDupont@ens.psl.eu; Khan_compu@emich.edu

Abstract. UV and O3 synergistic processes can effectively remove low concentrations of new pollutants in water, but the deep degradation of low concentrations of new pollutants needs further study. It was found that UV254/O3 treatment of phenol, SMX, and TC at low concentration (0.2 mmol·L-1) for 2 min resulted in a degradation rate of more than 90%, which was significantly higher than ATZ and CIP. There was a significant linear relationship between electronegativity (χ) and degradation rate constant (kobs) (Y = 6.086X - 20.339; R2 = 0.946). ROS quantitative experiments demonstrated that the electronic structures of these new pollutants could regulate the production of different reactive oxygen species (ROS) in the UV254/O3 system, and Phenol, SMX, and TC were positively correlated with the contents of superoxide anion (·O2-) and singlet oxygen (1O2). The toxicity test of Escherichia coli and the treatment experiment of municipal wastewater show that the UV254/O3 system has a good treatment effect on low-concentration new pollutants. This study reveals the treatment potential of UV254/O3 for new pollutants in practical water and provides a theoretical basis for the influence of different new pollutant structure characteristics on degradation rate.

Keywords: *UV254/O3, new pollutants, electronic structure, mechanistic studies, ROS modulation*

Received on 02 April 2025, Accepted on 25 April 2025, Published on 11 June 2025

1 Introduction

New pollutants are characterized by a wide variety, high toxicity, difficulty in biodegradation, and complex intermediates [1]. After entering the environment, they will direct or indirect affect the growth, development, and reproduction of organisms [2]. Prolonged persistence of emerging contaminants in aquatic systems poses grave risks to both ecological integrity and public health [3]. Currently, new pollutants in water are mainly removed by advanced oxidation technologies such as photocatalytic oxidation [4], electrocatalytic oxidation [5], peroxydisulfate (PDS)/peroxymonosulfate (PMS) activation [6-7], Fenton method [8-10], ozone method [11-12], and ultrasonic cavitation [13]. The UV–O_3 hybrid process stands out by merging photocatalytic and ozonation strengths to generate powerful oxidants such as hydroxyl radicals (·OH); these reactive oxygen species (ROS) facilitate the thorough decomposition and deep mineralization of pollutants. In addition, the UV/O_3 method also has a wide pH adaptability and no secondary pollution, making it a hot spot in new pollutant treatment technology [14].

Numerous studies have reported that the UV/O_3 system can efficiently degrade pollutants in water. For example, the ozone micro-nano bubble (O_3 (MNBs)) coupled with ultraviolet light enhancement process at pH = 9 produces ROS such as ·OH, which can rapidly degrade atrazine (ATZ) in water (98.7% degradation rate in 10 min) [15]; the TiO_2 photocatalytic ozonation process (O_3/UVA/TiO_2) produces ·OH and superoxide anion radicals ($\cdot O_2^-$), which can deeply mineralize ciprofloxacin (CIP) in water, with COD and TOC removal rates as high as 92.3% and 81.1% within 60 min [16]. However, current research on the UV/O_3 system mainly focuses on single new pollutants. Considering that there are many types of new pollutants in actual water bodies and their concentrations are low, usually in the range of 0.01 mmol·L^{-1} to 0.2 mmol·L^{-1} [18], and different new pollutants may have different degradation rates due to different molecular structures. Therefore, it is necessary to study

the combined degradation of multiple new pollutants by the UV/O_3 method, especially the treatment potential of low-concentration compound new pollutants, which remains to be studied.

The deep degradation of new pollutants extremely depends on the type and content of ROS generated in the system. Properties of new pollutants [17-18], reaction time [19], solution pH [20-23], and ionic strength [24] all affect the type of ROS, among which the properties of new pollutants have a significant impact on their own removal rate. For example, the degradation activity of Fe-NCv-900 catalyst with carbon vacancies for 7 phenolic pollutants increases with the decrease of electronegativity of substituents on the benzene ring of the pollutants [25]. The properties of new pollutants can also affect the contribution rate of different types of ROS in the degradation process, thereby affecting their own degradation rate constant. Studies have shown that the degradation efficiency of new pollutants with different structural characteristics in the $Co_{1.5}Ca_{1.5}Al_1$-LDO/PMS system varies significantly. Bisphenol A (BPA) (k_{obs} = 0.291 min^{-1}) and bisphenol B (BPB) (k_{obs} = 0.343 min^{-1}) containing electron-donating groups -CH_3 have significantly higher k_{obs} in this system than bisphenol S (BPS) (k_{obs} = 0.101 min^{-1}) [26]. Therefore, whether the removal efficiency of low-concentration new pollutants by UV/O_3 technology is related to the properties of new pollutants remains unknown.

This paper investigated the degradation kinetics of UV_{254}/O_3 synergistic process on 5 new pollutants (ATZ, sulfamethoxazole (SMX), CIP, phenol, tetracycline (TC)), explored the relationship between the properties of new pollutants and the degradation rate constant k_{obs} and their influence on ROS production in the system. The contribution of ROS generated in different systems to the degradation of new pollutants was explored, and the quantitative relationship between ROS generated by different new pollutants in the UV_{254}/O_3 system was clarified. In addition, the toxicity of the system before and after UV_{254}/O_3 treatment was evaluated by toxicity test of *Escherichia coli* (DHB4), proving that UV_{254}/O_3 technology can be applied to the advanced treatment of urban wastewater. This study provides theoretical guidance and practical solutions for the UV_{254}/O_3 advanced oxidation technology to treat new pollutants in water, and provides a certain reference for the regulation of ROS by the properties of new pollutants.

2 Materials and Methods

2.1 Experimental equipment and reagents

Experimental equipment: full-wavelength ultraviolet spectrophotometer (UV-8000), high performance liquid chromatograph (Waters e2695 Separations Module) with ultraviolet detector (2489 UV/Vis Detector), column C_{18} 5 μm (4.6 mm × 250 mm), 3D-EEM fluorescence spectrometer (F-4600 fluorescence spectrophotometer, Hitachi, Japan), ozone generator (CHUAVG), ozone concentration tester (3S-J5000), 254 nm ultraviolet lamp (UVGO), Leici (PHB-5) portable pH meter, KQ-500DE numerical control ultrasonic cleaner, and electric constant temperature blast drying oven (DHG-9053AD), etc.

Reagents: atrazine (ATZ), sulfamethoxazole (SMX), ciprofloxacin (CIP), phenol, tetracycline (TC), *p*-benzoquinone (BQ), benzoic acid (BA), furfuryl alcohol (FFA), nitroblue tetrazolium chloride (NBT), nitrobenzene (NB), sodium hydroxide, hydrochloric acid were all analytical grade. *Escherichia coli* DHB4 strain was stored in our laboratory at -80 °C. Ultrapure water (18.25 MΩ·cm) was used for all experiments.

2.2 Experimental methods

2.2.1 Degradation experiment

200 mL of 0.2 mmol·L^{-1} new pollutant (ATZ, SMX, CIP, TC and Phenol) was placed in a quartz ozone reactor (500 mL) and exposed to 254 nm UV irradiation and 1 mg·L^{-1} ozone atmosphere. Specifically, the combined UV–O_3 strategy harnesses the benefits of both photocatalytic and ozonation technologies, generating highly oxidative reactive oxygen species—most notably hydroxyl radicals (·OH)—that enable efficient contaminant breakdown and thorough mineralization.

Residual concentrations of the target contaminants were quantified by high-performance liquid chromatography (Agilent) on a Waters Symmetry C18 column (4.6 mm × 250 mm, 5 μm). The analytical conditions comprised a 20 μL injection volume, a column temperature of 30 °C, and a mobile-phase flow rate of 1 mL min^{-1}. Chromatographic separations were achieved with the following eluent systems and detection wavelengths: atrazine (ATZ), methanol/water (65:35, v/v) at 280 nm; sulfamethoxazole (SMX), acetonitrile/0.1 % acetic acid (60:40, v/v) at 257 nm; ciprofloxacin (CIP) and tetracycline (TC), acetonitrile/0.1 % formic acid (60:40, v/v) at 280 nm and 360 nm, respectively; and phenol, acetonitrile/water (60:40, v/v) at 280 nm.

2.2.2 Electronegativity calculation

The electronegativity (χ, eV) of organic molecules was calculated by the formula: χ = (IP + EA)/2, and the ionization potential (IP, eV) was calculated using equations (1) and (2).

$IP = E(M^+) - E(M)$ (1)

$EA = E(M) - E(M^-)$ (2)

Among them, E(M), $E(M^-)$, and $E(M^+)$ are the energies of neutral, anionic, and cationic states calculated by coupling the B3LYP/6-31+G(d,p) molecule with the solute electron density (SMD) model.

2.2.3 Trapping experiment

ROS trapping agents were added to the above 5 new pollutant systems, including NB (0.05 $mmol·L^{-1}$) trapping ·OH, NBT (0.01 $mmol·L^{-1}$) trapping $·O_2^-$, and FFA (1 $mmol·L^{-1}$) trapping $^1O_2$. The respective roles of individual radicals in eliminating emerging pollutants under UV_{254}/O_3 conditions were probed by introducing three scavengers and gauging their suppressive effects on contaminant breakdown [27].

2.2.4 Quantitative experiment

Kinetically, steady-state ROS levels were inferred from probe-compound decay trajectories. Nitrobenzene (NB) and furfuryl alcohol (FFA) were accordingly adopted to gauge the steady-state concentrations of ·OH and $^1O_2$, respectively. The steady-state concentration expressions are (3) and (4) [18]:

$d[NB]/dt = k_{NB,·OH}[NB][·OH]_{SS} = k_{NB}[NB]$ (3)

$[·OH]_{SS} = k_{NB}/k_{NB,·OH}$ (4)

In the formula, k_{NB} is the pseudo-first-order rate constant of NB decay. $k_{NB,·OH}$ (3.9×10^9 $(mol·L^{-1})^{-1}·s^{-1}$).

To determine the steady-state concentration of singlet oxygen ($^1O_2$), the analogous kinetic protocol was followed with furfuryl alcohol (FFA) substituted for nitrobenzene (NB) and $^1O_2$ in place of hydroxyl radicals. Probe concentrations were quantified by HPLC [28]. For NB, analysis was conducted at 265 nm using a mobile phase of 60 % acetonitrile and 40 % aqueous 0.1 % acetic acid (v/v) at 30 °C with a flow rate of 1.0 mL min^{-1}. The FFA assay used 216 nm, a methanol/water eluent (40:60, v/v), and identical temperature and flow conditions. Specific experimental operation: add NBT (2 mL, 1 $mmol·L^{-1}$) to the reaction solution (200 mL, 0.2 $mmol·L^{-1}$), stir well, expose the above suspension to 254 nm UV lamp and 1 $mg·L^{-1}$ ozone atmosphere, react for 3 min. During the reaction, take 4 mL solution every 30 s and filter. The obtained supernatant was measured with a UV-Vis spectrophotometer.

2.2.5 Toxicity assessment

To prove the toxicity removal ability of UV/O_3 technology on 5 $μmol·L^{-1}$ ATZ solution, *Escherichia coli* (DHB4) was used to monitor the toxicity of the degradation solution. The antibacterial toxicity was evaluated by colony

forming unit (CFU) of DHB4 [29]. For the antibacterial assay, DHB4 was first propagated to the exponential growth phase and the cell suspension was standardised to an optical density of 0.4 at 600 nm. Ninety microlitres of this inoculum were introduced into two separate vessels: one containing 9 mL of pristine 5 μmol L^{-1} ATZ solution and another containing 9 mL of ATZ solution pre-treated with UV/O_3 for 30 min. Both mixtures were incubated at 37 °C for 16 h. After exposure, serial dilutions were prepared, spread onto LB nutrient agar, and colony-forming units were enumerated following an overnight incubation. All test equipment was sterilized in an autoclave at 121 °C before use.

2.2.6 Three-dimensional fluorescence spectrum analysis of urban wastewater

Three-dimensional excitation–emission matrix (3D-EEM) fluorescence spectroscopy was employed to characterise dissolved organic matter (DOM) in raw municipal wastewater as well as in effluents subjected to UV_{254} and UV_{254}/O_3 treatment. Spectra were recorded on an F-4600 fluorescence spectrophotometer (Hitachi, Japan) by scanning emission wavelengths from 250 to 550 nm in 5 nm increments, while excitation was stepped from 220 to 450 nm at the same interval, using a scan speed of 1200 nm min^{-1}. A distilled-water spectrum acquired under identical settings served as the blank.

Fluorescence intensity in EEM analysis typically increases with dissolved organic matter levels. The EEM map is divided into five regions: Regions I–II denote aromatic protein-like compounds, Region III fulvic acid analogues, Region IV benzene-containing proteins and soluble microbial by-products, and Region V humic acid analogues [30].

3 Results and Discussion

3.1 Relationship between degradation efficiency of UV254/O3 system and electronic properties of new pollutants

3.1.1 Degradation effect of UV254/O3 system on different new pollutants

The degradation of 5 low-concentration (0.2 mmol·L^{-1}) new pollutants by UV_{254}/O_3 technology is shown in Figure 1. After 2 min of reaction, the degradation rates of ATZ, CIP, Phenol, SMX, and TC in the UV_{254}/O_3 system were 26%, 32%, 87%, 92%, and 99% (Figure 1a). The first-order kinetic fitting curve shows that the reaction rates of new pollutants in UV_{254}/O_3 were k_{ATZ} (0.1111 min^{-1}) < k_{CIP} (0.1800 min^{-1}) < k_{Phenol} (0.6575 min^{-1}) < k_{SMX} (1.0520 min^{-1}) < k_{TC} (3.6174 min^{-1}). It can be seen that the degradation efficiency of different new pollutants in the UV_{254}/O_3 system varies significantly, but the specific reasons for this difference still need further study.

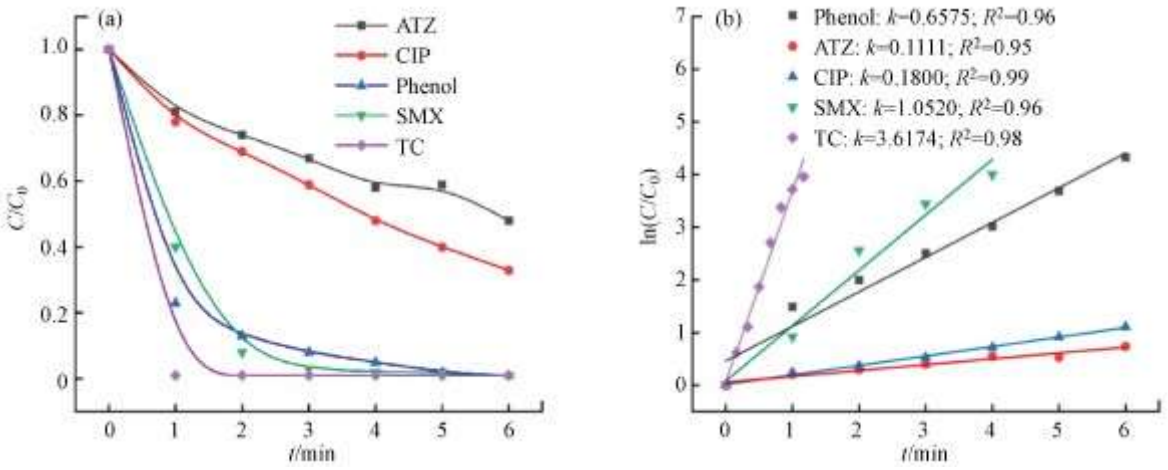

Figure 1 (a) Degradation kinetics of different new pollutant in UV254/O3 system; (b) First-order kinetic fitting curve

DOI:

3.1.2 Effect of new pollutant properties on kobs

To rationalise the divergent degradation behaviour of the five emerging contaminants in the UV_{254}/O_3 system, their quantum-chemical descriptors were correlated with the observed rate constants ($k_{o\beta s}$). Accordingly, density functional theory was employed to compute ionisation potentials (IP), electron affinities (EA), nucleophilic indices (NI) and electronegativities (χ) for each pollutant (Table 1). Correlation analysis was performed between the k_{obs} of new pollutants and their corresponding electronic property descriptors. It can be seen that the k_{obs} of new pollutants has no obvious linear relationship with IP, EA, and NI (Figure 2abc). It is worth noting that the k_{obs} of new pollutants has a strong linear correlation with χ (Y = 6.086X - 20.339; R^2 = 0.946) (Figure 2d) (from large to small: TC (3.90215) > SMX (3.59335) > Phenol (3.45) > CIP (3.3714) > ATZ (3.3189)). The results show that the χ of new pollutants is positively correlated with their k_{obs}, indicating that the electronic properties of new pollutants can significantly affect their degradation efficiency in the UV_{254}/O_3 system, and the larger the χ, the higher the degradation efficiency. However, the mechanism by which the χ of new pollutants affects degradation efficiency is still unclear.

Table 1 Electronic property descriptors for new contaminants

	IP/eV	EA/eV	NI	χ
TC	7.5037	0.3006	3.1586	3.90215
SMX	7.913	-0.7267	2.8214	3.59335
Phenol	6.09	0.81	3.1513	3.45
CIP	7.0866	-0.3438	3.5395	3.3714
ATZ	8.178	-1.5402	2.7118	3.3189

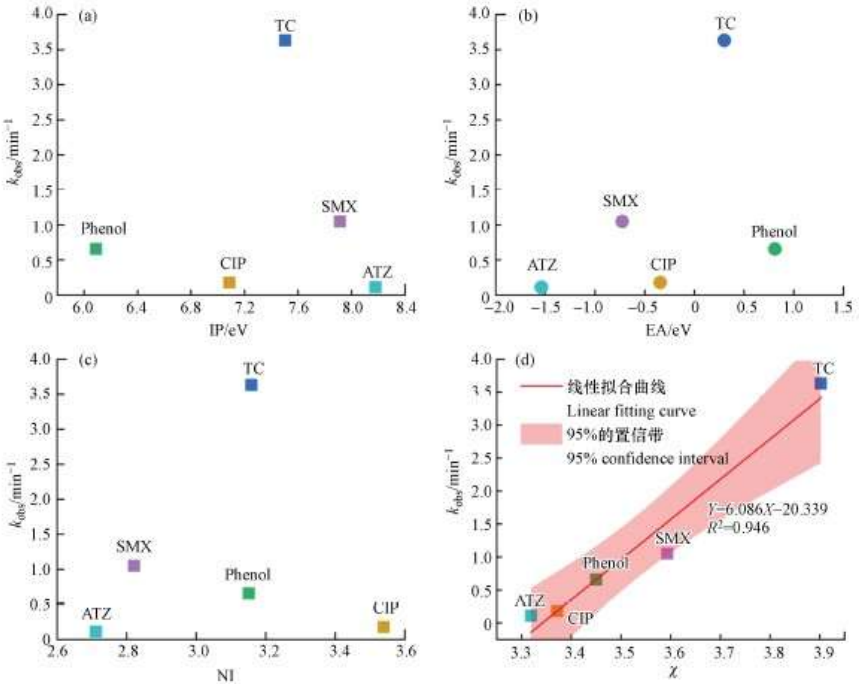

Figure 2 (a) Different new pollutant IP vs. kobs; (b) Different new pollutant EA vs. kobs; (c) Different new pollutant NI vs. kobs; (d) Different new pollutant χ vs. kobs.

3.2 Dominant regulation of new pollutants on ROS

3.2.1 Effect of new pollutants on ROS types

Based on the above analysis, to further explore the mechanism of how the χ of new pollutants affects degradation efficiency, NB, NBT, and FFA were used to capture ·OH, $\cdot O_2^-$, and $^1O_2$ produced by different pollutants in the UV_{254}/O_3 system. The regulation of new pollutant χ on ROS in the UV_{254}/O_3 system was explored through the inhibitory effect of trapping agents on the removal of new pollutants. Figure 3a reveals that TC breakdown was strongly hindered by both NB and NBT. FFA likewise exerted a marked suppressive effect, driving the degradation rate constant down from 1.11082 min^{-1} to 0.37867 min^{-1}. Therefore, when TC was used as the substrate in the UV_{254}/O_3 system, $^1O_2$ was the dominant ROS. The inhibitory trends of NB, NBT, and FFA on the degradation of SMX and ATZ were consistent, with the inhibitory effect of ·OH < $\cdot O_2^-$ < $^1O_2$ (Figure 3(be)). Therefore, when SMX and ATZ were used as substrates in the UV_{254}/O_3 system, the contribution of the three ROS was ·OH < $\cdot O_2^-$ < $^1O_2$. The addition of NB, NBT, and FFA all inhibited the degradation of Phenol and CIP, among which the inhibitory effect of FFA was much higher than that of NB and NBT, while NB was slightly higher than NBT (Figure 3(cd)). Therefore, when Phenol and CIP were used as substrates for degradation in the UV_{254}/O_3 system, the contribution of ROS was $\cdot O_2^-$ < ·OH < $^1O_2$. It can be seen that in the UV_{254}/O_3 system, although the χ of new pollutants did not directly affect the type of ROS, the contribution rate of different new pollutants to ROS varied significantly, which may be related to the production of ROS. However, it is still unclear whether the χ of new pollutants affects the production of ROS.

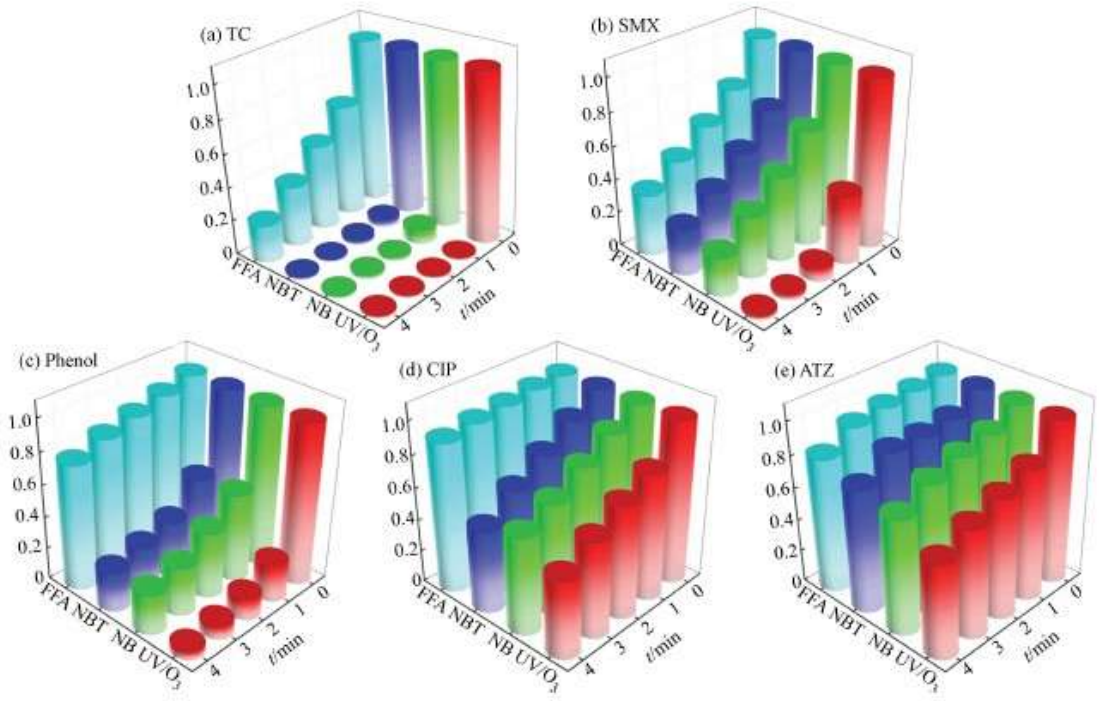

Figure 3 (a) different capture agents on TC degradation rate; (b) different capture agents on SMX degradation rate; (c) different capture agents on Phenol degradation rate; (d) different capture agents on CIP degradation rate; (e) different capture agents on ATZ degradation rate (Experimental conditions: [O3]0 = 2 mg·L-1, pH = 6.78, V = 200 mL, [substrate]0 = 0.1 mmol·L-1, [NBT] = 0.01 mmol·L-1, [NB] = 0.05 mmol·L-1, [FFA] = 1 mmol·L-1)

3.2.2 Effect of new pollutant χ on ROS production

Nitrobenzene was utilized as a molecular probe to track hydroxyl-radical (·OH) generation, thereby elucidating how the electronegativity (χ) of various emerging contaminants influences ·OH production. The steady-state ·OH

DOI:

concentration ($[\cdot OH]_{ss}$) was subsequently derived from the pseudo-first-order decay rate constant (k_{nB}) of nitrobenzene according to the relationship given in Equations 3 and 4 (Table 2). The pseudo-first-order rates of NB decay were $k_{TC\text{-}NB}$ = 0.19 min^{-1}, $k_{SMX\text{-}NB}$ = 0.21 min^{-1}, $k_{Phenol\text{-}NB}$ = 0.33 min^{-1}, $k_{CIP\text{-}NB}$ = 0.25 min^{-1}, $k_{ATZ\text{-}NB}$ = 0.07 min^{-1} (Figure 4a). Accordingly, the ·OH production was in the order of Phenol (1.41 × 10^{-12} mol·L^{-1}) > CIP (1.07 × 10^{-12} mol·L^{-1}) > SMX (8.90 × 10^{-13} mol·L^{-1}) > TC (8.13 × 10^{-13} mol·L^{-1}) > ATZ (3.00 × 10^{-13} mol·L^{-1}). Therefore, the ·OH production of TC, SMX, and CIP was inversely proportional to χ.

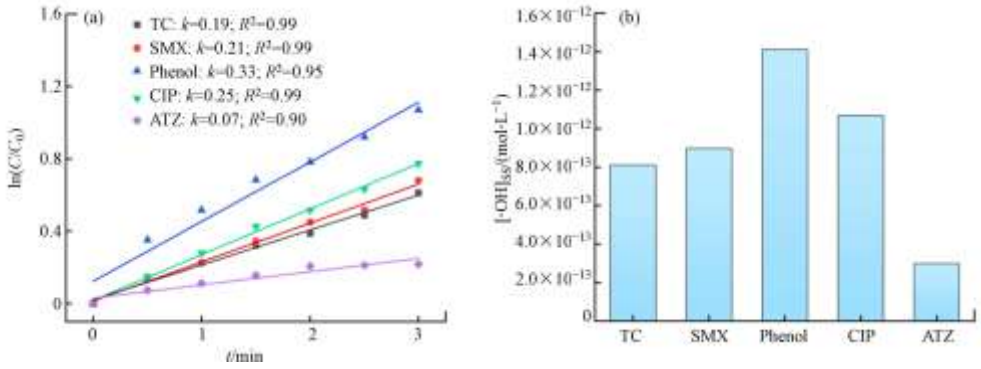

Figure 4 Fig.4 (a) Comparison of pseudo-first-order rates of NB decay under different new pollutant; (b) Comparison of steady-state concentration of hydroxyl radicals [-OH]SS under different new pollutant (Experimental conditions: [O3]0 = 1 mg·L-1, pH = 6.78, [NBT]0 = 0.01 mmol·L-1, V = 200 mL)

Table 2 The k_{NB} and $[\cdot OH]_{SS}$ under different substrate conditions in the UV_{254}/O_3 system

	k_{NB}/min^{-1}	$[\cdot OH]_{SS}$/(mol·L^{-1})
TC	0.19	8.13 × 10^{-13}
SMX	0.21	8.90 × 10^{-13}
Phenol	0.33	1.41 × 10^{-12}
CIP	0.25	1.07 × 10^{-12}
ATZ	0.07	3.00 × 10^{-13}

NBT was used as a probe for $\cdot O_2^-$ to explore the effect of different new pollutant χ on $\cdot O_2^-$ production. The results are shown in Figure 5. The production rates of $\cdot O_2^-$ were k_{TC} = 3.15 min^{-1}, k_{SMX} = 2.47 min^{-1}, k_{Phenol} = 0.19 min^{-1}, k_{CIP} = 1.35 min^{-1}, k_{ATZ} = 0.09 min^{-1}. Therefore, the $\cdot O_2^-$ production of TC, SMX, and CIP was positively correlated with χ.

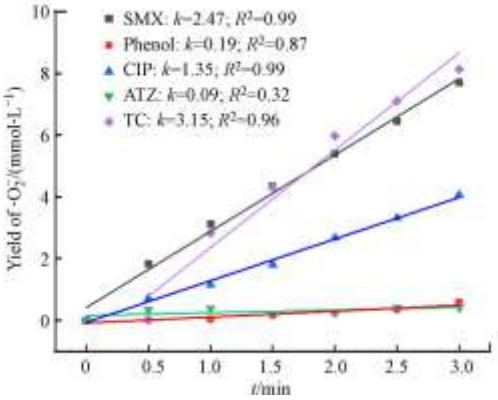

Figure 5 Effects of different new pollutant on ·O2- production

DOI:

FFA was used as a probe for $^1O_2$ to explore the effect of different new pollutant χ on $^1O_2$ production. The steady-state concentration $[^1O_2]_{SS}$ was calculated through the relationship between the pseudo-first-order kinetic constant k_{FFA} of FFA decay and $[^1O_2]_{SS}$. The results are shown in Table 3 and Figure 6. In the UV_{254}/O_3 system, the pseudo-first-order rates of FFA decay for different new pollutants were $k_{TC\text{-}FFA}$ = 1.499 min^{-1}, $k_{SMX\text{-}FFA}$ = 0.693 min^{-1}, $k_{Phenol\text{-}FFA}$ = 0.495 min^{-1}, $k_{CIP\text{-}FFA}$ = 0.511 min^{-1}, $k_{ATZ\text{-}NB}$ = 0.739 min^{-1}. It can be seen from Figure 6(b) that when 5 new pollutants were degraded in the UV_{254}/O_3 system, the $^1O_2$ production was TC (2.08×10^{-10} mol·L^{-1}) > ATZ (1.03×10^{-10} mol·L^{-1}) > SMX (9.62×10^{-11} mol·L^{-1}) > CIP (7.10×10^{-11} mol·L^{-1}) > Phenol (6.87×10^{-11} mol·L^{-1}). Among them, the $^1O_2$ production of TC, SMX, and CIP during degradation in UV_{254}/O_3 was positively correlated with χ. Because $^1O_2$ is the precursor of O_2 formation [31], the generation of $^1O_2$ is produced by the reaction of O_2 with H_2O or ·OH or H (reaction equations (5-7)). Therefore, the $^1O_2$ production is positively correlated with the $\cdot O_2^-$ production.

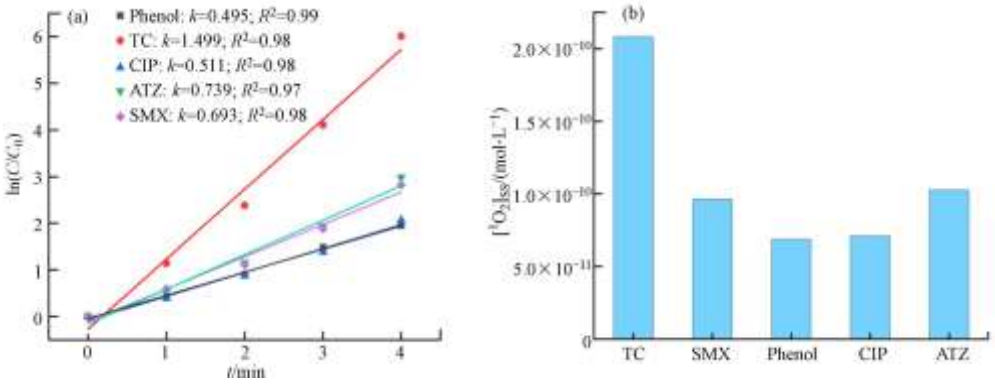

Figure 6 (a) Comparison of pseudo-first-order rates of FFA decay with different new pollutant; (b) Effect of different new pollutant on 1O2 production (Experimental conditions: [O3]0 = 1 mg·L−1, pH = 6.78, [FFA]0 = 1 mmol·L−1, [substrate]0 = 0.2 mmol·L−1and V = 200 mL)

Table 3 k_{FFA} and $[^1O_2]_{SS}$ under different new pollutant in the UV_{254}/O_3 system

	k_{FFA}/min^{-1}	$[^1O_2]_{SS}$/(mol·L^{-1})
TC	1.499	2.08×10^{-10}
SMX	0.693	9.62×10^{-11}
Phenol	0.495	6.87×10^{-11}
CIP	0.511	7.10×10^{-11}
ATZ	0.739	1.03×10^{-10}

$\cdot O_2^- + 2H_2O \rightarrow {}^1O_2 + H_2O_2 + 2OH^-$ (5)

$\cdot O_2^- + OH\cdot \rightarrow {}^1O_2 + OH^-$ (6)

$2\cdot O_2^- + 2H^+ \rightarrow {}^1O_2 + H_2O_2$ (7)

As reported elsewhere [32], phenol deviates from the general trend because ozonation of phenolics generates superoxide radicals ($\cdot O_2^-$) via two parallel routes: radical-chain propagation and ozone decomposition. Specifically, reaction (8) illustrates that ozone adds electrophilically to the aromatic ring, yielding HO_2^-; this intermediate then fragments through cleavage of its labile O–O bond to release $\cdot O_2^-$ [33]. Moreover, $\cdot O_2^-$ acts as a critical intermediate en route to hydroxyl radicals [34]; equations (9) and (12) [35] depict how radical-chain sequences convert $\cdot O_2^-$ into ·OH, akin to the transformations involving $HO_2\cdot$ and $HO_3\cdot$ shown in reactions (9) and (10) [36]. It can be seen that while the Phenol radical conversion pathway has ·OH → $\cdot O_2^-$ → $^1O_2$, there is also $\cdot O_2^-$ → ·OH, so Phenol is the largest in OH quantification, and the smallest in $\cdot O_2^-$ and $^1O_2$ quantification. The reason

DOI:

for ATZ exception is the influence of solution pH during the reaction and the electronic characteristics of ATZ. When pH = 9, O_3 mainly produces ·OH [37] (Figure 7a), and when pH = 7, it mainly produces $\cdot O_2^-$ (Figure 7b). In addition, the $^1O_2$ production is not affected by pH (Figure 7(c)). Therefore, when ATZ is the substrate, the $^1O_2$ production is relatively high. In addition, ATZ, as an electron-deficient body, lacks easily available electrons in its molecular structure, making it difficult to be oxidized. This means that the characteristics of ATZ have little effect on its ability to absorb UV or react with O_3, so its χ has no direct relationship with the production of ROS. In contrast, electron-rich pollutants such as TC and SMX, because they easily provide electrons, promote O_3 decomposition to produce ROS, thus showing a significant linear relationship with ROS production. Therefore, compared with other new pollutants, the removal efficiency of Phenol and ATZ is not suitable to be explained by their χ.

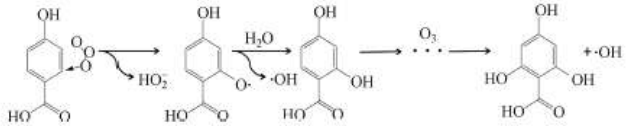

(8)

$\cdot O_2^- + O_3 \rightarrow O_3^- + O_2$ (9)

$O_3 + HO_2^- \rightarrow \cdot OH + O_2 + \cdot O_2^-$ (10)

$HO_3\cdot \rightarrow \cdot OH + O_2$ (11)

In summary, the χ of TC, SMX, and CIP is positively correlated with the production of $\cdot O_2^-$ and $^1O_2$, and negatively correlated with the production of ·OH, which indicates that the χ of new pollutants can regulate the production of ROS, affecting the degradation rate of new pollutants in the UV_{254}/O_3 system by increasing the ability of the UV_{254}/O_3 system to produce $\cdot O_2^-$ and $^1O_2$.

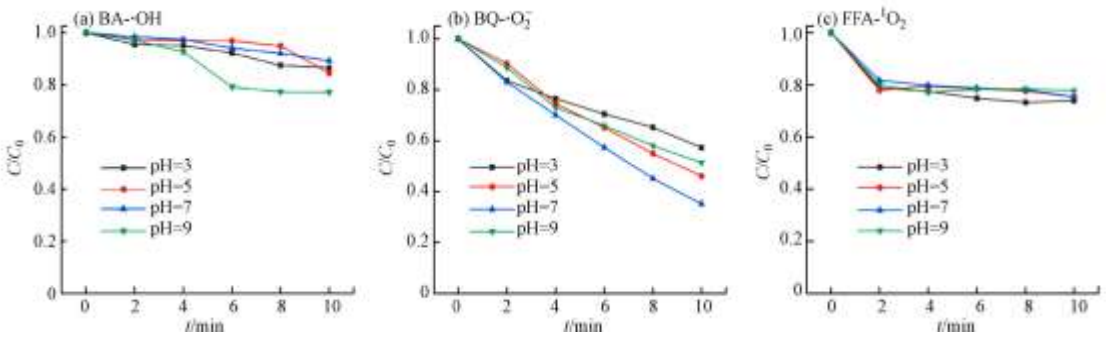

Figure 7 Free radical trapping experiments at different pH (Experimental conditions: [O3]0 = 5 mg·L−1, pH = 3, 5, 7, 9, V = 300 mL, [trapping agent]0 = 5 mmol·L−1 and [ATZ]0 = 0.3 mg·L−1)

3.3 Treatment Potential

Through the quantitative analysis of ROS production in different new pollutant systems, the specific mechanism of ROS regulation by the properties of new pollutants was clarified. On this basis, this study further evaluated the practical treatment potential of the UV254/O3 system for low-concentration compound new pollutants. First, by monitoring the growth of DHB4 colonies in the degradation solution, and using the most difficult-to-degrade ATZ as the substrate, the toxicity removal ability of the UV254/O3 process for new pollutants was investigated. The potential toxicity of ATZ solutions before and after UV254/O3 treatment was evaluated by colony forming units (CFU) of DHB4. The results showed that after dilution by a factor of 105 and plating for counting, the number of Escherichia coli in the untreated ATZ solution was 3, while the number of Escherichia coli in the treated ATZ solution was 123 (Figure 8). It can be seen that even at a concentration of only 5 μmol·L-1, the untreated ATZ solution almost completely inhibited Escherichia coli, showing strong toxicity. In contrast, Escherichia coli could grow in the treated ATZ solution, with almost no toxicity. The UV254/O3 system exhibited high degradation efficiency in the treatment of low-concentration new pollutants.

DOI:

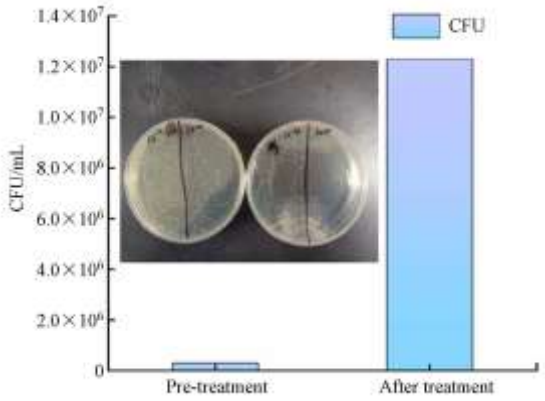

Figure 8 Comparison of toxicity of ATZ before and after treatment with UV254/O3 ozone (Experimental conditions: 5 μmol·L-1, Treatment time: 30 min)

Further exploration was conducted on the advanced treatment capability of UV254/O_3 technology for municipal domestic sewage that may contain multiple low-concentration new pollutants. 3D-EEM fluorescence spectroscopy was used to detect the dissolved organic matter in untreated urban wastewater, urban wastewater treated only with UV254, and urban wastewater treated with UV254/O_3. As shown in Figure 9(a), the untreated urban wastewater had fluorescence intensity in all five regions. The fluorescence intensity in Region I was weak, indicating that the urban wastewater contained a small amount of the first type of aromatic protein-like substances. The fluorescence intensity in Regions II and III was strong, indicating that the urban wastewater contained a large amount of the second type of aromatic protein-like substances and fulvic acid-like substances. The fluorescence intensity in Regions IV and V was the strongest, indicating that the urban wastewater contained a large amount of proteins containing benzene rings, soluble microbial by-products, and humic acid-like substances. Figure 9(b) shows the urban wastewater treated with UV254 alone for 5 min. The fluorescence intensity in each region was slightly reduced compared to the untreated urban wastewater, and except for Region I, the fluorescence intensity in the other regions remained very strong. Figure 9(c) shows the fluorescence spectrum of urban wastewater after 1 min of UV254/O_3 treatment. It can be seen from the figure that the fluorescence intensity in all regions was very weak, indicating that the treatment effect of UV254/O_3 on urban wastewater was more significant than that of UV254 alone. UV254/O_3 not only has the characteristics of being green and environmentally friendly like UV254, but also has much higher efficiency than UV254 alone. Therefore, the UV254/O_3 system can completely degrade organic pollutants in urban domestic wastewater with only 1 min of treatment.

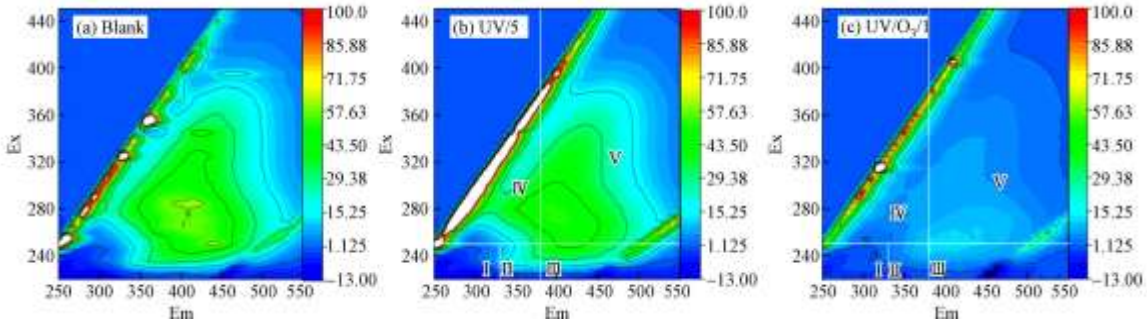

Figure 9 (a) Untreated urban wastewater; (b) Urban wastewater after UV254 treatment for 5 min; (c) Urban wastewater after 1 min of UV254/O3 treatment (Experimental conditions: [O3]0 = 10 mg·L-1 and V = 400 mL)

4 Conclusion

This paper studied the deep degradation ability of UV_{254}/O_3 technology on 5 low-concentration new pollutants. It was found that the 3 ROS (·OH, $\cdot O_2^-$, and $^1O_2$) generated by the UV_{254}/O_3 system played a role in the degradation process of these 5 new pollutants, and the contribution of ROS was related to the electronic properties of new pollutants. For TC, SMX, and ATZ, the contribution of different ROS was ·OH < $\cdot O_2^-$ < $^1O_2$; for Phenol and CIP, it was $\cdot O_2^-$ < ·OH < $^1O_2$. In addition, the amount of ROS produced by different new pollutants under neutral conditions also varied. The ·OH production was in the order of Phenol > CIP > SMX > TC > ATZ, the $\cdot O_2^-$ production rate was $k_{TC} > k_{SMX} > k_{CIP} > k_{Phenol} > k_{ATZ}$, and the $^1O_2$ production was TC > ATZ > SMX > CIP > Phenol. Except for Phenol and ATZ, among the other 3 pollutants, the production of $\cdot O_2^-$ and $^1O_2$ was positively correlated with the χ of new pollutants, while the production of ·OH was negatively correlated with the χ of new pollutants. Changes in pH value significantly affected the production of ·OH and $\cdot O_2^-$. The ·OH production was the largest at pH = 9, and the $\cdot O_2^-$ production was the highest at pH = 7, while the $^1O_2$ production was almost unaffected by pH value. Finally, the toxicity test of *Escherichia coli* and the experiment of urban domestic wastewater proved that the toxicity of the pollutant solution after UV_{254}/O_3 treatment was greatly reduced, and low-concentration organic pollutants could be efficiently removed in only 1 min.

References

[1] LIU G L, XU C X. About the "organic micropollutants" in groundwater [J]. Scientific and Cultural Popularization of Land and Resources, 2020(3): 26-29 (in Chinese).

[2] HUANG K C, ZHAO Z, HOAG G E, et al. Degradation of volatile organic compounds with thermally activated persulfate oxidation [J]. Chemosphere, 2005, 61(4): 551-560.

[3] YU Y N, GU Y H, HUANG J W, et al. Characteristics and ecological risk assessment of typical micropollutants in the urban storm sewer system [J]. Guangdong Chemical Industry, 2022, 49(7): 119-121 (in Chinese).

[4] ANTONOPOULOU M, KOSMA C, ALBANIS T, et al. An overview of homogeneous and heterogeneous photocatalysis applications for the removal of pharmaceutical compounds from real or synthetic hospital wastewaters under lab or pilot scale [J]. Science of the Total Environment, 2021, 765: 144163.

[5] MARTINEZ-HUITLE C A, PANIZZA M. Electrochemical oxidation of organic pollutants for wastewater treatment [J]. Current Opinion in Electrochemistry, 2018, 11: 62-71.

[6] DING Y, WANG X, FU L, et al. Nonradicals induced degradation of organic pollutants by peroxydisulfate (PDS) and peroxymonosulfate (PMS): Recent advances and perspective [J]. Science of the Total Environment, 2021, 765: 142794.

[7] YANG S, WANG P, YANG X, et al. A novel advanced oxidation process to degrade organic pollutants in wastewater: Microwave-activated persulfate oxidation [J]. Journal of Environmental Sciences, 2009, 21(9): 1175-1180.

[8] MORONE A, MULAY P, KAMBLE S P. Removal of pharmaceutical and personal care products from wastewater using advanced materials [J]. Pharmaceuticals and personal care products: waste management and treatment technology, 2019: 173-212.

[9] JIANG J, WANG X, LIU Y, et al. Photo-Fenton degradation of emerging pollutants over Fe-POM nanoparticle/porous and ultrathin g-C3N4 nanosheet with rich nitrogen defect: Degradation mechanism, pathways, and products toxicity assessment [J]. Applied Catalysis B: Environmental, 2020, 278: 119349.

[10] LACSON C F Z, DE LUNA M D G, DONG C, et al. Fluidized-bed Fenton treatment of imidacloprid: Optimization and degradation pathway [J]. Sustainable Environment Research, 2018, 28(6): 309-314.

[11] MALIK S N, GHOSH P C, VAIDYA A N, et al. Hybrid ozonation process for industrial wastewater treatment: Principles and applications: A review [J]. Journal of Water Process Engineering, 2020, 35: 101193.

[12] WANG J, WANG S. Reactive species in advanced oxidation processes: Formation, identification and reaction mechanism [J]. Chemical Engineering Journal, 2020, 401: 126158.

[13] LEE Y, SEDLAK D L, VON GUNTEN U. Oxidative water treatment: The track ahead [J]. Environmental Science & Technology, 2023, 57(47): 18391-18392.

[14] PAN Z H. Mechanism and dynamics of photocatalytic-ozone combined degradation of organic pollutants [D]. Wuhan: Huazhong University of Science and Technology, 2013 (in Chinese).

[15] CHEN L Y. Efficacy of atazine with ozone micro-nano bubble coupled UV enhancement in water [D]. Harbin: Harbin Institute of Technology, 2022 (in Chinese).

[16] ASGARI E, SHEIKHMOHAMMADI A, NOURMORADI H, et al. Degradation of ciprofloxacin by photocatalytic ozonation process under irradiation with UVA: Comparative study, performance and mechanism [J].

Process Safety and Environmental Protection, 2021, 147: 356-366.
[17] HUANG R, GAO P, ZHU J, et al. Insights into the pollutant electron property inducing the transformation of peroxymonosulfate activation mechanisms on manganese dioxide [J]. Applied Catalysis B: Environmental, 2022, 317: 121753.
[18] ZHANG M, RUAN J, WANG X, et al. Selective oxidation of organic pollutants based on reactive oxygen species and the molecular structure: Degradation behavior and mechanism analysis [J]. Water Research, 2023, 246: 120697.
[19] DAI C M, JIA C Y, HU J J, et al. Research progress on mechanism and influencing factors of advanced oxidation technology with peracetic acid [J]. Industrial Water Treatment, 2023, 43(1): 1-9 (in Chinese).
[20] HUANG X, REN W, LIU X, et al. CuMgFe-LDO as superior peroxymonosulfate activator for imidacloprid removal: Performance, mechanism and effect of pH [J]. Chemical Engineering Journal, 2022, 441: 136135.
[21] ZHOU Z, ZENG H, LI L, et al. Methyl contributes to the directed phosphorus doping of g-C3N4: PH-dependent selective reactive oxygen species enable customized degradation of organic pollutants [J]. Water Research, 2024, 255: 121521.
[22] CHEN X J, BAI C W, SUN Y J, et al. pH-driven efficacy of the ferrate(VI)-peracetic acid system in swift sulfonamide antibiotic degradation: A deep dive into active species evolution and mechanistic insights [J]. Environmental Science & Technology, 2023, 57(48): 20206-20218.
[23] CHU Y, XU M, LI X, et al. Oxidation of emerging contaminants by S(IV) activated ferrate: Identification of reactive species [J]. Water Research, 2024, 251: 121100.
[24] LIU Y C, YANG B, LI Q M, et al. Effects and mechanism of Cl- and pH on organic matter removal in salt-containing wastewater treatment by advanced oxidation processes [J]. Chinese Journal of Environmental Engineering, 2021, 15(5): 1487-1499 (in Chinese).
[25] WEI S, SUN Y, QIU Y Z, et al. Self-carbon-thermal-reduction strategy for boosting the Fenton-like activity of single Fe-N4 sites by carbon-defect engineering [J]. Nature Communications, 2023, 14(1): 7549.
[26] XIE Z H, HE C S, ZHOU H Y, et al. Effects of molecular structure on organic contaminants' degradation efficiency and dominant ROS in the advanced oxidation process with multiple ROS [J]. Environmental Science & Technology, 2022, 56(12): 8784-8795.
[27] YIN R, SHANG C. Removal of micropollutants in drinking water using UV-LED/chlorine advanced oxidation process followed by activated carbon adsorption [J]. Water Research, 2020, 185: 116297.
[28] CHENG S, ZHANG X, YANG X, et al. The multiple role of bromide ion in PPCPs degradation under UV/chlorine treatment [J]. Environmental Science & Technology, 2018, 52(4): 1806-1816.
[29] LIU H, QU J, ZHANG T, et al. Insights into degradation pathways and toxicity changes during electro-catalytic degradation of tetracycline hydrochloride [J]. Environmental Pollution, 2020, 258: 113702.
[30] XIE L, JIANG Z C, ZHAO M F, et al. Research and application of fluorescence spectroscopy in water quality detection [J]. Water Resources Research, 2023, 12(3): 238-245 (in Chinese).
[31] LEE W J, BAO Y, GUAN C, et al. Ce/TiOx-functionalized catalytic ceramic membrane for hybrid catalytic ozonation-membrane filtration process: Fabrication, characterization and performance evaluation [J]. Chemical Engineering Journal, 2021, 410: 128307.
[32] WANG Z, LIN X, HUANG Y, et al. The role of hydroxylation on ·OH generation for enhanced ozonation of benzoic acids: Reactivity, ozonation efficiency and radical formation mechanism [J]. Journal of Hazardous Materials, 2022, 431: 128620.
[33] STAEHELIN J, HOIGNE J. Decomposition of ozone in water in the presence of organic solutes acting as promoters and inhibitors of radical chain reactions [J]. Environmental Science & Technology, 1985, 19(12): 1206-1213.
[34] WANG Y, CAO H, CHEN L, et al. Tailored synthesis of active reduced graphene oxides from waste graphite: Structural defects and pollutant-dependent reactive radicals in aqueous organics decontamination [J]. Applied Catalysis B: Environmental, 2018, 229: 71-80.
[35] SEHESTED K, HOLCMAN J, HART E J. Rate constants and products of the reactions of e-aq, dioxide(1-)(O2-) and proton with ozone in aqueous solutions [J]. The Journal of Physical Chemistry, 1983, 87(11): 1951-1954.
[36] ZHANG J, ZHANG Y L, SHI Y N, et al. Acceleration of ozone decomposition and ·OH generation by hydroxylamine [J]. Ozone: Science & Engineering, 2016, 38(2): 150-155.
[37] ELOVITZ M S, VON GUNTEN U, KAISER H P. Hydroxyl radical/ozone ratios during ozonation processes. II. the effect of temperature, pH, alkalinity, and DOM properties [J]. Ozone: Science & Engineering, 2000, 22(2): 123-150.